

## Article

# Domain-Adaptive Framework for ACL Injury Diagnosis Utilizing Contrastive Learning Techniques

Weiqiang Liu <sup>1,2</sup> , Weilun Lin <sup>3</sup> , Zefeng Zhuang <sup>4</sup> and Kehua Miao <sup>3,\*</sup> <sup>1</sup> School of Computer Science, Minnan Normal University, Zhangzhou 363000, China; lwq2688@mnnu.edu.cn<sup>2</sup> Key Laboratory of Data Science and Intelligence Application, Fujian Province University, Zhangzhou 363000, China<sup>3</sup> Department of Automation, Xiamen University, Xiamen 361000, China<sup>4</sup> Department of Computer Science, University of Bristol, Bristol BS8 1QU, UK

\* Correspondence: zxkd@xmu.edu.cn

**Abstract:** In sports medicine, anterior cruciate ligament (ACL) injuries are common and have a major effect on knee joint stability. For the sake of prognosis evaluation and treatment planning, an accurate clinical auxiliary diagnosis of ACL injuries is essential. Although existing deep learning techniques for ACL diagnosis work well on single datasets, research on cross-domain data transfer is still lacking. Building strong domain-adaptive diagnostic models requires addressing domain disparities in ACL magnetic resonance imaging (MRI) from different hospitals and making efficient use of multiple ACL datasets. This work uses the publicly available KneeMRI dataset from Croatian hospitals coupled with the publicly available MRnet dataset from Stanford University to investigate domain adaptation and transfer learning models. First, an optimized model efficiently screens training data in the source domain to find unusually misclassified occurrences. Subsequently, before being integrated into the contrastive learning module, a target domain feature extraction module processes features of target domain samples to improve extraction efficiency. By using contrastive learning between positive and negative sample pairs from source and target domains, this method makes domain adaptation easier and improves the efficacy of ACL auxiliary diagnostic models. Utilizing a spatially augmented ResNet-18 backbone network, the suggested approach produces notable enhancements in experimentation. To be more precise, the AUC for transfer learning improved by 3.5% from MRnet to KneeMRI and by 2.5% from KneeMRI to MRnet (from 0.845 to 0.870). This method shows how domain transfer can be used to improve diagnostic accuracy on a variety of datasets and effectively progresses the training of a strong ACL auxiliary diagnostic model.

**Keywords:** anterior cruciate ligament; convolutional neural network; contrastive learning; domain adaptation



**Citation:** Liu, W.; Lin, W.; Zhuang, Z.; Miao, K. Domain-Adaptive Framework for ACL Injury Diagnosis Utilizing Contrastive Learning Techniques. *Electronics* **2024**, *13*, 3211. <https://doi.org/10.3390/electronics13163211>

Academic Editors: Yifeng Zeng, Yingke Chen and Xu Wang

Received: 15 July 2024

Revised: 11 August 2024

Accepted: 12 August 2024

Published: 14 August 2024



**Copyright:** © 2024 by the authors. Licensee MDPI, Basel, Switzerland. This article is an open access article distributed under the terms and conditions of the Creative Commons Attribution (CC BY) license (<https://creativecommons.org/licenses/by/4.0/>).

## 1. Introduction

The knee joint [1] functions as a hinge joint and is stabilized by four key ligaments. These ligaments [2] are essential for connecting bones and regulating joint movements. The knee is supported by two collateral ligaments on its sides and two cruciate ligaments within the joint. The cruciate ligaments, namely the anterior cruciate ligament (ACL) [3] and the posterior cruciate ligament (PCL) [4], connect the distal end of the femur to the proximal end of the tibia. Figure 1 provides a detailed illustration of the knee joint's anatomical structure.

The anterior cruciate ligament (ACL) is a crucial component of the knee joint, connecting the femur to the tibia. It is one of the most vulnerable ligaments in the human body and frequently sustains injuries that often necessitate surgical repair [5]. ACL tears are the most prevalent type of knee injury [6]. Given the intricate structure of the knee joint, the ACL is essential for maintaining stability and function. Consequently, prompt and precise diagnosis and treatment of ACL injuries are critically important.

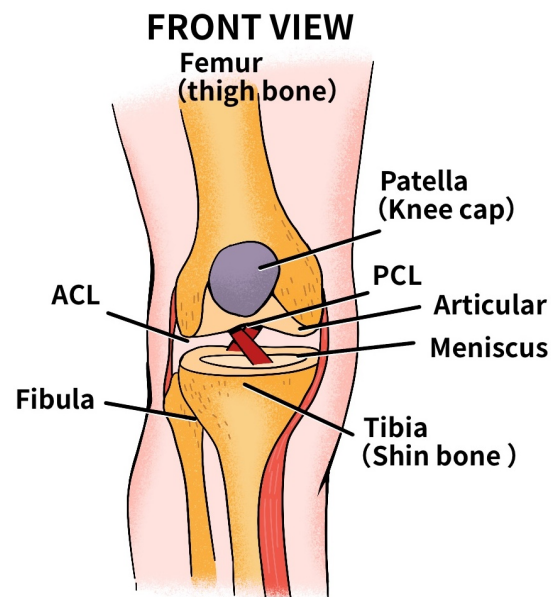


**Figure 1.** The structure of the knee joint.

ACL tears are among the most common knee injuries, with an incidence rate in the United States reaching up to 74.6% [7]. These injuries are particularly prevalent among athletes, especially those involved in soccer, basketball, and volleyball. The rising awareness of health and the growing number of sports participants have led to an annual increase in ACL injury cases [8]. Research indicates that ACL injuries significantly compromise knee stability and adversely impact patients' quality of life [9–12]. Hence, timely and precise diagnosis, along with effective treatment, is essential for managing ACL injuries.

Current clinical methods for diagnosing ACL injuries predominantly involve various imaging techniques [13–15], including ultrasound, computed tomography (CT), and magnetic resonance imaging (MRI). While ultrasound and CT can present challenges in accurately localizing injuries, MRI is regarded as the preferred diagnostic tool. MRI excels in clearly depicting the structures and tissue changes within the knee joint, making it particularly advantageous for diagnosing ACL injuries. Consequently, MRI is extensively utilized in clinical settings for the assessment of ACL damage.

In recent years, the widespread application of deep learning technology [16–22] has led to significant advancements in medical imaging, particularly in diagnosing ACL injuries. Bien et al. developed the MRnet dataset and employed ImageNet transfer learning weights to train multiple AlexNet networks to detect ACL tears, meniscal tears, and other injuries [23]. Their model, validated using the external KneeMRI dataset by Stajduhar et al., achieved an area under the curve (AUC) of 91%, markedly surpassing previous results [24]. Awan et al. redesigned the ResNet14 architecture based on the KneeMRI dataset, focusing on ACL injury diagnosis. By using hybrid class balancing and real-time data augmentation strategies, they addressed class imbalance issues and achieved a three-class accuracy (ACC) of 92% [25]. Recent studies have introduced the lightweight ELNet model, which, when combined with multi-scale normalization and blur pooling techniques, achieved an AUC of 96% for ACL tear detection on the MRnet dataset [26]. Dunnhofer et al. employed a pyramid feature model to extract the local region of interest (ROI) area of each MRI slice, increasing the AUC for ACL injury detection to 97.6% [27]. Additionally, Belton et al. used spatial attention and feature concatenation techniques to enhance the model's ability to capture critical features within each MRI slice, achieving an AUC of 97.2% [28]. These studies highlight the immense potential of deep learning in medical imaging diagnostics, paving the way for more accurate diagnosis of ACL injuries.

Despite tremendous advances in applying deep learning to diagnose ACL injuries, some hurdles remain, most notably dataset variety and sample distribution heterogeneity.

These limitations impede models' generalization capabilities, reducing their performance in real-world clinical contexts. Domain adaptation and transfer learning systems present promising solutions to these problems. By utilizing knowledge transfer from one domain to another, these technologies can improve model performance on new datasets while also effectively managing changes between datasets. Domain adaptation approaches allow information to be transferred across source and target domains, even when there are large data distribution disparities. These strategies can increase model correctness and resilience, eliminate the requirement for huge volumes of labeled data in settings with few annotations, and reduce data gathering costs and time. This study investigates and utilizes domain adaptation and transfer learning strategies to solve the limitations of current ACL injury diagnosis models. By combining these advanced methodologies, we hope to improve diagnostic model accuracy and reliability across a wide range of datasets and clinical settings. This strategy will give more effective and practical tools for medical practice, hence increasing patient diagnosis and treatment outcomes while also advancing medical imaging diagnostics.

This study uses the MRnet and KneeMRI datasets to model MRI images using advanced deep learning methods. By combining these datasets, we provide source and target domain data, allowing for successful domain adaptation and transfer learning for ACL damage detection. This method improves the model's generalization performance across multiple data circumstances. This work also provides useful reference material for ACL domain transfer models and has potential implications in clinical auxiliary diagnostics. The primary contributions of this study are as follows:

(i) This is the first study to investigate domain adaptation and transfer learning for ACL diagnosis utilizing the MRnet and KneeMRI datasets. The suggested strategy overcomes the limits of single-dataset models by improving generalization performance across a variety of data circumstances.

(ii) We provide a novel source and target domain data processing technique based on contrastive learning, which yields a one-to-many domain adaption framework. This approach aligns the feature distributions in the source and target domains, making it better suited to the study's specific requirements.

(iii) The experimental results, using a ResNet-18 backbone and a spatial attention mechanism, reveal that our contrastive learning-based domain transfer strategy outperforms both fine-tuned and hybrid training models.

The remaining sections of this work are organized as follows. Section 2 summarizes relevant work on transfer learning models and feature transfer approaches. Section 3 describes the proposed technique. Section 4 explains the datasets and experimental methodologies in depth. Finally, Section 5 summarizes the findings and suggests areas for future investigation.

## 2. Related Work

### 2.1. ACL Transfer Learning Model

Bien et al. [23] compiled a dataset of 1370 MRI samples from Stanford University Hospital Center, representing the largest publicly available knee database to date. This dataset includes MRI images from three perspectives: sagittal, coronal, and axial views. Using the AlexNet architecture and pre-trained ImageNet parameters, Bien et al. [23] trained nine different models across these three MRI views to detect ACL tears, meniscal tears, and other abnormalities.

The final ACL confidence in Bien et al.'s method is derived by training ACL models from three different views and then combining their confidence scores using logistic regression. This approach effectively utilizes model fusion techniques. For the external dataset KneeMRI, curated by Stajduhar et al. [24], it only includes MRI data from the sagittal view. Initially, Bien et al. [23] tested the KneeMRI dataset using the sagittal ACL model from MRnet, achieving an AUC of 82.4%. Due to these results not meeting expectations, Bien et al. [23] reorganized the KneeMRI dataset into training, validation, and test sets in a

6:2:2 ratio. Subsequently, they applied transfer learning by initializing the model parameters with MRnet's pre-trained weights. This adaptation led to a significant improvement, achieving an AUC of 91.1%, outperforming the previous study [24].

It is evident that Bien et al. [23], despite applying transfer learning to the KneeMRI dataset, did not fully capitalize on the additional coronal and axial information available in MRnet. Essentially, their approach focused on transferring knowledge from a single view (sagittal) to another single view (sagittal). The potential benefits of incorporating coronal and axial data to enhance the guidance of the KneeMRI dataset warrant further investigation.

## 2.2. Feature Transfer

One of the most used approaches to medical image analysis is model-based transfer learning, especially for image classification tasks. This method makes use of pre-trained models, such as various traditional deep convolutional neural networks (DCNNs), built on ImageNet. The key benefit of this technique is the use of models with high classification accuracy, which eliminates the need for significant model pre-training. In classification jobs, there is a widespread preference for changing the pre-trained model's fully connected (FC) layers for classification purposes rather than using approaches such as support vector machines. This strategy is preferred because it enables the use of a single model for both feature extraction and classification, making model deployment more convenient and efficient.

In medical image analysis, feature-based transfer learning is pivotal, especially in scenarios where the features of source and target domain data either do not overlap or only partially overlap. When there is feature overlap, the approach involves learning mapping functions to align data from the source and target domains into a unified feature space. This process helps mitigate inter-domain disparities. For instance, techniques like feature space transformation transfer learning [29] and scale-invariant feature transformation transfer learning [30] have proven highly effective in addressing these challenges. They facilitate the adaptation of models by transforming features across domains, thereby enhancing the model's capability to generalize across different datasets and clinical scenarios.

In cases where features between domains do not overlap, transfer learning requires mechanisms to convert between these distinct feature spaces. Research has demonstrated the efficacy of cross-domain kernel learning techniques, such as the domain transfer support vector machine (SVM) method proposed by Cheng et al. [31]. This approach involves mapping auxiliary domains and target domains into a reproducing kernel Hilbert space (RKHS) and constructing new kernel functions to minimize differences in data distribution between domains. This method has shown promising results in applications like the classification of mild cognitive impairment converters (MCI-Cs) and non-converters (MCI-NCs), illustrating its effectiveness in adapting models across disparate datasets and improving classification accuracy.

Furthermore, feature space transformation (FST) methods have proven advantageous in mitigating feature representation disparities arising from variations in scanners or scanning parameters. For example, Opbroek et al. [29] employed the FST method in MRI brain image segmentation studies. They carried this out by generating unlabeled source-target sample pairs and linking labeled training samples to the nearest  $k$  source samples. This approach effectively addresses differences in feature reconstruction between training and test data sets.

Despite the widespread applicability and benefits of feature-based transfer learning in medical image analysis, a number of problems remain. For example, determining domain invariance becomes more difficult when dealing with labeled data, whereas acquiring generalizable features across domains might be difficult in the absence of labeled data. As research continues to address these issues, feature-based transfer learning is expected to play an increasingly important role in the advancement of medical image analysis.



### 3. Proposed Method

#### 3.1. Framework

Bien et al. [23] utilized the MRnet model for transfer learning on the KneeMRI dataset by fine-tuning the model, but without explicitly considering the relationship between samples from different domains. In clinical practice, MRI equipment varies across hospitals, resulting in distributional differences in data. Consequently, models trained on source domain data may not generalize well to target domain data. Therefore, there is a critical need to develop more sophisticated domain adaptation methods for ACL diagnosis. These methods should leverage the relationships between features from source and target domains to facilitate effective transfer of knowledge to target domain data.

This study introduces a contrastive learning-based domain-adaptive model for ACL diagnosis. By employing contrastive learning between samples from the source and target domains, the disparity between domains is minimized. Figure 2 illustrates the key steps of the proposed approach. The architecture consists of two main components: model training and data preprocessing.

The data preparation procedure is divided into two major tasks: feature extraction from the target domain and sample filtering in the source domain. During the filtering phase, the model predicts the source domain samples, and those that are mistakenly classified are then processed. Meanwhile, samples from the target domain are processed by the model's backbone network to extract features that are then used to calculate the contrastive loss.

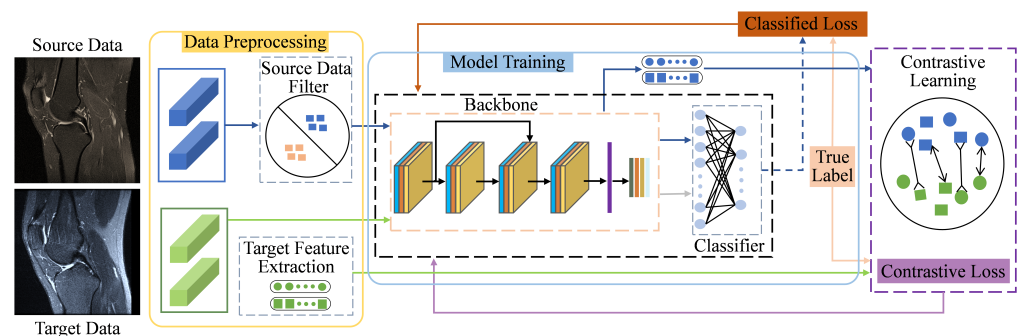


**Figure 2.** The framework of the main methods.

During the model training phase, samples from both the source and target domains are used as inputs. For the target domain samples, only the classification cross-entropy loss is calculated. In contrast, for the source domain samples, in addition to the classification cross-entropy loss, the contrastive loss is calculated using the target domain-extracted features.

The network used in the workflow consists of two parts: a feature extraction network and a classifier network. The MRI data are in the form of  $N \times 3 \times H \times W$ , where  $N$  represents the number of slices for the sample and  $H, W$  represents the image size. The feature extraction network converts this into a  $1 \times 1000$  vector through a backbone network, average pooling, fully connected layers, and max pooling. The classifier network, composed of fully connected layers and a sigmoid activation function, then predicts the probability of the vector belonging to the positive class.

The upcoming sections will offer a comprehensive description of the specific components within the framework.

#### 3.2. Data Preprocessing

##### 3.2.1. Source Data Filter

In contrastive learning, positive samples are those that belong to the same class as the anchor sample, while negative samples belong to different classes. The main idea is to move positive and negative samples around in the feature space, bringing positive samples closer to the anchor sample and pushing negative samples away. A correct prediction

suggests that the sample is more closely aligned with the positive samples of the target domain in feature space. An inaccurate prediction happens when the model, which has been fine-tuned for the target domain, places the sample closer to negative samples while predicting source domain samples. To bring wrongly classified samples closer to positive samples, remedial measures are required. The detailed process is illustrated in Figure 3.

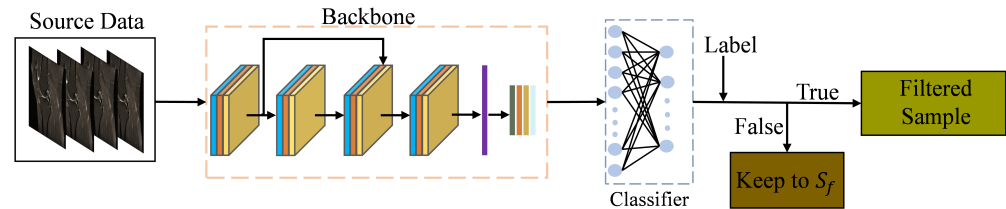


**Figure 3.** The framework of source data filtering.

Our experimental strategy includes testing the model on the entire source domain dataset before each training iteration. Samples that are misclassified—where the model’s predictions do not align with the actual labels—are gathered into a set  $S_f$ . This set is then combined with the target domain training set for subsequent training iterations. The detailed process is outlined in Algorithm 1.

The essence of this strategy is to guide the misclassified source domain samples so that the model can update their feature representations during training. This modification seeks to better align the feature distributions of the source and target domains. By correcting these misclassified samples, the difference in distribution between the source and target domains can be successfully reduced, improving the model’s performance in the target domain.

---

#### Algorithm 1 Source Data Filter

---

**Require:** Source training set  $S$ , Source training set labels  $Y_S$ , Network  $G$

**Ensure:** Misclassified samples  $S_f$

```

1:  $S_f \leftarrow \emptyset$                                 ▷ Initialize the set of misclassified samples
2: for  $(x, y) \in (S, Y_S)$  do
3:    $\hat{y} \leftarrow G(x)$                             ▷ Predict label using network  $G$ 
4:   if  $\hat{y} \neq y$  then
5:      $S_f \leftarrow S_f \cup \{x\}$                 ▷ Add misclassified sample to  $S_f$ 
6:   end if
7: end for
8: return  $S_f$ 

```

---

#### 3.2.2. Target Feature Extraction

In traditional contrastive learning methods, the practice involves placing an equal number of source domain and target domain samples into a single batch for training. However, the unique format ( $N \times C \times H \times W$ ) of MRI dataset samples typically results in each batch containing only one source domain sample and one target domain sample. This setup presents challenges for the direct implementation of contrastive learning. Alternatively, conducting real-time feature extraction for all target domain samples and calculating contrastive loss with the current source domain sample during each training step would be highly time-consuming. This approach could significantly impact the experiment’s efficiency and feasibility. The detailed process is illustrated in Figure 4.

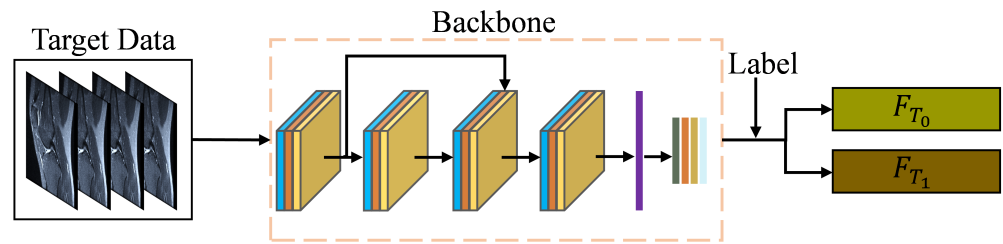


**Figure 4.** The framework of target feature extraction.

To tackle this challenge, we adopted a more streamlined and time-efficient experimental approach. Prior to each training iteration, we began by utilizing the model to extract features from the target domain training set. Subsequently, based on the sample labels, we partitioned the target domain features into two distinct sets:  $F_{T_0}$  and  $F_{T_1}$ . These sets were then utilized in the subsequent training iteration for calculating contrastive loss alongside the source domain samples. The detailed process is outlined in Algorithm 2.

This preprocessing technique enabled us to extract and organize the target domain's features before training began. This allowed us to bypass the batch size constraint and use pre-extracted features for contrastive learning computations while training. Furthermore, our technique dramatically reduces processing costs by eliminating the need for repeated feature extraction in each training session. This change increases the practicality and efficiency of employing contrastive learning on MRI data.

---

**Algorithm 2** Target Feature Extraction

---

**Require:** Target training set  $T$ , Target training set labels  $Y_T$ , Feature extraction network  $G'$   
**Ensure:** Target class 0 feature set  $F_{T_0}$ , Target class 1 feature set  $F_{T_1}$

1: $F_{T_0} \leftarrow \emptyset$	▷ Initialize the feature set for class 0
2: $F_{T_1} \leftarrow \emptyset$	▷ Initialize the feature set for class 1
3: <b>for</b> $(x, y) \in (T, Y_T)$ <b>do</b>	
4: $f \leftarrow G'(x)$	▷ Extract features using network $G'$
5: <b>if</b> $y = 0$ <b>then</b>	
6: $F_{T_0} \leftarrow F_{T_0} \cup \{f\}$	▷ Add features to class 0 feature set
7: <b>else if</b> $y = 1$ <b>then</b>	
8: $F_{T_1} \leftarrow F_{T_1} \cup \{f\}$	▷ Add features to class 1 feature set
9: <b>end if</b>	
10: <b>end for</b>	
11: <b>return</b> $F_{T_0}, F_{T_1}$	

---

### 3.3. Contrastive Learning

In the previous section, we discussed employing several data preprocessing methodologies for source and target domain MRI data to optimize their participation in contrastive learning. The challenge remains how to successfully train the preprocessed data. To address this, we propose utilizing different loss calculation methods during training based on whether the data are from the source or target domain. This method enables us to make the best use of label information in a supervised contrastive learning framework while also effectively exploiting inter-domain information.

For the target domain data, the model computes the classification loss using the cross-entropy loss function. The specific formula is depicted below, where  $p$  denotes the predicted probability of the positive class, and  $y$  represents the actual label.

$$loss_{Target} = H(p, y) = -y \log(p) - (1 - y) \log(1 - p) \quad (1)$$

For the source domain data, the model also calculates the contrastive loss relative to the target domain data. This method facilitates bringing the source domain data closer to the target domain data within the feature space.

Specifically, the target domain features and source domain features are initially paired as positive and negative samples. Each current source domain feature, paired with each corresponding same-class target domain feature, constitutes a positive sample pair. Conversely, each current source domain feature, paired with each different-class target domain feature, forms a negative sample pair. Here,  $F_i^{Sf}$  represents the feature extracted from the  $i$ -th filtered source domain sample by the network.  $F_{T_0}$  and  $F_{T_1}$  represent the feature vector sets of the two classes in the target domain extracted during preprocessing.  $F^+$  denotes the set of target domain positive sample features corresponding to  $F_i^{Sf}$ , and  $F^-$  denotes the set of target domain negative sample features corresponding to  $F_i^{Sf}$ .  $|F^+|$  and  $|F^-|$  represent the number of positive and negative sample pairs in the sets, respectively.

For each positive and negative sample pair, we first calculate their cosine similarity using the following formula:

$$r(a, b) = \frac{a^T b}{\|a\| \|b\|} \quad (2)$$

Next, the cosine similarity is divided by the hyperparameter  $\tau$  and exponentiated. Subsequently, the InfoNCE (Noise Contrastive Estimation) loss function is computed, and the mean value is derived as the final loss.

$$loss_{InfoNCE} = -\frac{1}{|F^+|} \sum_{k=1}^{|F^+|} \log \left( \frac{\phi(F_i^{Sf}, F_k^+)}{\phi(F_i^{Sf}, F_k^+) + \sum_{j=1}^{|F^-|} \phi(F_i^{Sf}, F_j^-)} \right) \quad (3)$$

$$\phi(a, b) = \exp\left(\frac{r(a, b)}{\tau}\right) \quad (4)$$

The final contrastive loss is weighted and added to the classification loss of the target domain to compute the overall loss. The specific formula is as follows, where  $\lambda$  is a hyperparameter:

$$loss_{Source} = H(p, y) + \lambda loss_{InfoNCE} \quad (5)$$

To leverage the intrinsic knowledge in target domain samples, a supervised classification loss function is used. For source domain samples, a hybrid technique of classification loss and contrastive loss is used. This strategy takes advantage of both the intrinsic properties of the source domain and the inter-domain information exchanged with the destination domain. As a result, it changes the distribution of source and target domain samples within the feature space, increasing the similarity of source domain samples to those from the target domain. This method tries to increase the model's performance in the target domain by efficiently combining contrastive learning and MRI data.

## 4. Experiments and Results

This section details the materials and procedures used in the investigation. Section 4.1 discusses the MRI image dataset and details the data pretreatment processes. Following that, Section 4.2 describes the experimental setting and the assessment metrics employed. Section 4.3 presents the experimental data and analyses.

### 4.1. Dataset

#### 4.1.1. KneeMRI Dataset

The initial dataset utilized in this study originated from the Rijeka Clinical Hospital Center [28] and is known as the KneeMRI dataset. It includes knee MRI scans from 917 patients, categorized into 690 healthy cases, 172 with partial tears, and 55 with complete tears. Healthy samples are labeled as 0, partial tears as 1, and complete tears as 2.

#### 4.1.2. MRnet Dataset

The second dataset utilized in this study was sourced from the Stanford University Medical Center [23] and is known as the MRnet dataset. This dataset comprises MRI scans from 1250 patients, with 988 classified as healthy and 262 showing signs of tears. Healthy samples are labeled as grade 0, while tear samples are labeled as grade 1. As depicted in Figure 5, each case includes MRI slice sequences captured in three orientations: the axial plane proton density-weighted series (PD), the coronal plane T1-weighted series, and the sagittal plane T2-weighted series. Each sequence in these orientations consists of 17 to 61 slices.

### 4.2. Experimental Design and Evaluation Metrics

#### 4.2.1. Experimental Design

To validate the efficacy of our proposed method, we employed the baseline model described by Belton et al. [28], which utilizes ResNet-18 [32] augmented with spatial attention mechanisms. Initially, the model was trained on the source domain data to establish a pre-trained baseline. The pre-trained model was then fine-tuned using solely the target domain data as a baseline comparison. We further investigated the model's performance by fine-tuning it across both the combined source and target domains. Following these steps, experiments involving contrastive learning were carried out with the model fine-tuned solely with target domain data.

Three views of MRI examination

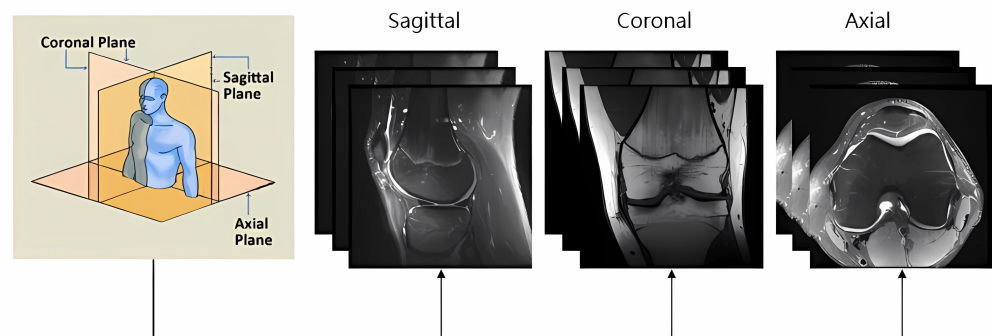


**Figure 5.** Three-view diagram of MRnet dataset.

Setting hyperparameters is a critical aspect of convolutional neural networks (CNN) model training as it significantly influences model performance. In this study, we initialized the learning rate to  $1 \times 10^{-5}$  and employed the Adam optimization method. Due to the specific properties of MRI dataset samples, the batch size was set to one. The source domain training phase lasted 50 epochs, while the subsequent experimental phases, such as fine-tuning and contrastive learning, lasted 20 epochs each. To ensure reproducibility, all tests were carried out with a random seed of 42. Our method makes use of Python within the PyTorch GPU framework to provide efficient computation.

To ensure consistency, we processed the KneeMRI dataset, which only contains sagittal plane data, and the MRnet dataset, which only has binary classification labels. In the KneeMRI dataset, classifications 1 (partial tear) and 2 (full tear) were combined into a single category, 1 (tear). We solely used sagittal plane data in the MRnet dataset. The two datasets were partitioned as detailed below to ensure fairness in comparing experiments.

Firstly, since the original authors [24] did not provide a standardized split for the dataset, we randomly split the KneeMRI dataset at the patient level. When the KneeMRI dataset was used as the source domain, the data were divided into training, validation, and testing sets in a 7:1:2 ratio. Conversely, when used as the target domain, the training and testing sets were swapped, resulting in a 2:1:7 ratio for training, validation, and testing.

Secondly, for the MRnet dataset, the original authors [23] had already split the data into training, validation, and testing sets. However, because the test set was not publically



available, we used the original validation set as the test set while resplitting the original training set into new training and validation sets. The new validation set contained the same number of samples as the new test set, and the healthy-to-injured ratio stayed balanced. When the source domain was employed, the training, validation, and testing sets had a ratio of about 8:1:1. Similarly, when the target domain was employed, the training and testing sets were swapped, yielding a training, validation, and testing ratio of 1:1:8. The dataset was processed using the histogram equalization technique [33] to correct for uneven pixel intensities in MRI sequences.

The primary objective of this experiment was to validate the effectiveness of the proposed contrastive learning method when using the KneeMRI dataset and the MRnet dataset as both source and target domains.

#### 4.2.2. Evaluation Metrics

The confusion matrix, shown in Figure 6, is crucial for evaluating model performance as it shows the relationship between true and predicted labels:

Confusion Matrix		Label	
		Positive	Negative
Predict	Positive	TP	FP
	Negative	FN	TN

**Figure 6.** Example of confusion matrix.

True Positive (TP): Correctly predicted positives.

False Negative (FN): True positives falsely predicted as negatives.

False Positive (FP): Actual negatives falsely predicted as positives.

True Negative (TN): Correctly predicted negatives.

We use the following metrics:

*Accuracy*: The proportion of correct predictions:

$$Accuracy = \frac{TP + TN}{TP + FP + TN + FN} \quad (6)$$

*Precision*: The proportion of true positives among predicted positives:

$$Precision = \frac{TP}{TP + FP} \quad (7)$$

*Recall*: The proportion of true positives that are correctly identified:

$$Recall = \frac{TP}{TP + FN} \quad (8)$$

*Specificity*: The proportion of actual negatives that are correctly identified:

$$Specificity = \frac{TN}{TN + FP} \quad (9)$$

*F<sub>1</sub> score*: The harmonic mean of precision and recall:

$$F_1 = 2 \times \frac{Precision \times Recall}{Precision + Recall} \quad (10)$$

In binary classification, a default threshold of 0.5 is frequently used to categorize data. However, the ideal threshold can vary. In this study, we determined the optimal threshold for the validation set before testing and applied it to classification. The generated confusion matrix was then utilized to determine the scoring measures.

To evaluate model performance independent of this criterion, we utilized AUC. The AUC measures the model's overall performance by comparing the true positive rate (TPR) versus the false positive rate (FPR) at various thresholds. It gives an overall score for the model's ability to differentiate across classes, with values ranging from 0 to 1.

TPR represents the proportion of actual positive samples that are correctly predicted as positive.

$$TPR = \frac{TP}{TP + FN} \quad (11)$$

FPR represents the proportion of actual negative samples that are incorrectly predicted as positive.

$$FPR = \frac{FP}{TN + FP} \quad (12)$$

To assess the model at different thresholds, we calculated the true positive rate (TPR) and false positive rate (FPR) and displayed them to create the Receiver Operating Characteristic (ROC) curve. In contrast to threshold measurements such as accuracy or  $F_1$  score, this curve provides a comprehensive view of model performance across all thresholds. We then used the area under the ROC curve (AUC), which ranged from 0 to 1, to evaluate the model's overall performance. Higher AUC values indicate improved discrimination. In this study, the AUC was the primary parameter for assessing and comparing model efficacy.

#### 4.3. Analysis of Experimental Results

To test the efficacy of contrastive learning, we ran comparison experiments using the MRnet and KneeMRI datasets, considering each as both the source and target domain. Samples with ruptured ligaments were uniformly classified as positive, whereas healthy samples were labeled as negative. To achieve fair comparisons, we used consistent data divisions and hyperparameters throughout the experiment.

Tables 1 and 2 show performance metrics for several strategies, including “fine-tuned”, “merged”, and the proposed methods.

**Table 1.** Comparison of transfer learning experiments from KneeMRI to MRnet.

Method	AUC	ACC	Precision	Recall	Specificity	$F_1$
Fine-Tuned [28]	0.8385	0.8099	0.6830	0.7680	0.8283	0.7062
Merged	0.8447	0.8347	0.6988	0.7507	0.8715	0.7184
Ours	0.8703	0.8693	0.7472	0.7338	0.9287	0.7402

**Table 2.** Comparison of transfer learning experiments from MRnet to KneeMRI.

Method	AUC	ACC	Precision	Recall	Specificity	$F_1$
Fine-Tuned [28]	0.8331	0.8422	0.7858	0.7966	0.8861	0.7909
Merged	0.8462	0.8375	0.8000	0.7290	0.9420	0.7532
Ours	0.8812	0.8828	0.8561	0.8149	0.9482	0.8324

The term “fine-tune” refers to the process of taking a pre-trained model from one dataset (source domain) and continuing its training on another dataset (target domain). The goal of this strategy is to adjust the model's learned features to the specific properties of the target domain, thus increasing its performance on the new dataset.

“Merge” refers to merging data from many sources or domains into a single training dataset. This strategy seeks to leverage the combined data's diversity and richness to increase the model's capacity to generalize across diverse types of input.

#### 4.3.1. Analysis of Overall Experimental Results

As depicted in Tables 1 and 2, we utilized both the MRnet and KneeMRI datasets, treating each as both source and target domains. The findings show that our contrastive learning strategy considerably improved the model's performance, resulting in optimal outcomes in transfer learning scenarios with small target dataset sizes. Notably, models trained by combining source and target domain training sets outperformed fine-tuned models. This demonstrates how useful insights from the source domain data can provide tasks to the target domain. It emphasizes the vital relevance of fully utilizing source domain data in knowledge transfer initiatives.

Specifically, in the transfer learning from KneeMRI to MRnet, the AUC increased from 0.845 to 0.870, marking a 2.5% improvement. Similarly, in the transfer learning from MRnet to KneeMRI, the AUC improved from 0.846 to 0.881, showing a 3.5% increase. The ROC curves depicted in Figure 7 vividly demonstrate these improvements in the AUC metric, affirming the substantial enhancement in model performance.

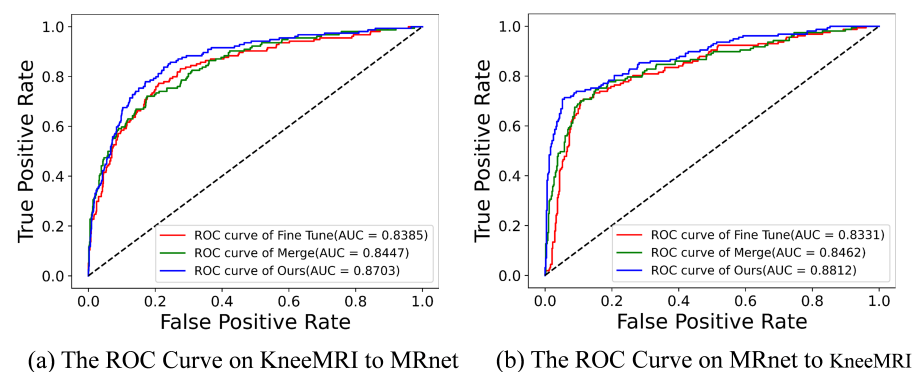


**Figure 7.** The ROC curve.

To further validate the effectiveness of the contrastive learning method, we utilized T-distributed Stochastic Neighbor Embedding (T-SNE) visualization to display the features extracted from the source and target domains. As depicted in Figure 8, compared to features generated by the pre-trained model, the fine-tuned model, and the model trained with merged datasets, the features extracted after contrastive learning demonstrated that the source domain features were more closely aligned with the distribution of positive samples in the target domain. This illustrates the feasibility and efficacy of contrastive learning in aligning features, effectively reducing the distribution gap between source and target domains.

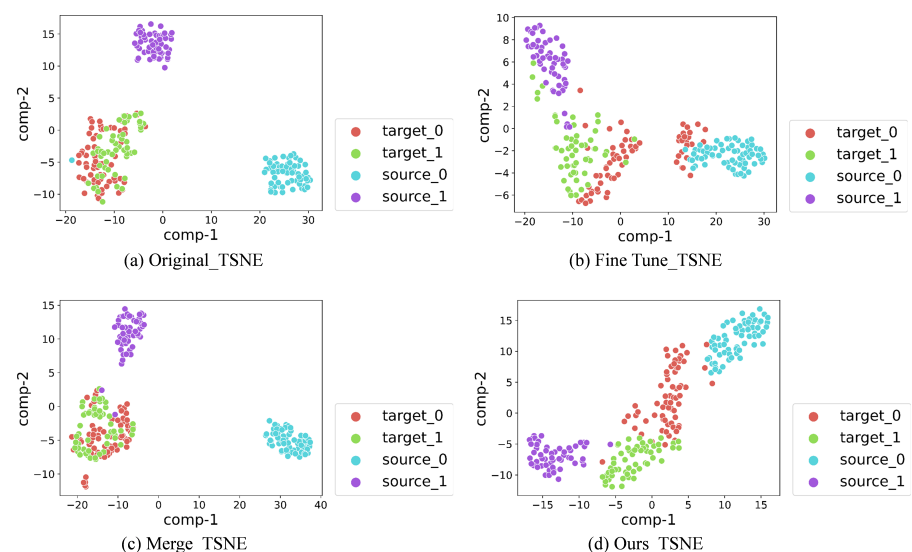


**Figure 8.** The tSNE figures. (a) Original. (b) Fine-tuned. (c) Merged. (d) Ours.

To summarize, the suggested strategy was thoroughly validated using bidirectional transfer experiments between the KneeMRI and MRnet datasets, resulting in significant improvements across all analyzed measures. The experimental results strongly support the method's usefulness and feasibility, notably in addressing the difficulty of weak generalization in ACL diagnostic models through contrastive learning. Furthermore, the findings of the bidirectional transfer experiment demonstrate the broad application of the suggested approach, giving useful insights and avenues for future study in medical picture detection models.

#### 4.3.2. Analysis of Hyperparameter Configuration Results

We conducted experimental tests with varying configurations of the hyperparameter  $\lambda$  to comprehensively assess the robustness and performance of the proposed method. Here,  $\lambda$  denotes the weight assigned to the contrastive loss, influencing the emphasis placed on contrastive learning during the training of target domain samples. The results of these experiments are depicted in Figure 9.

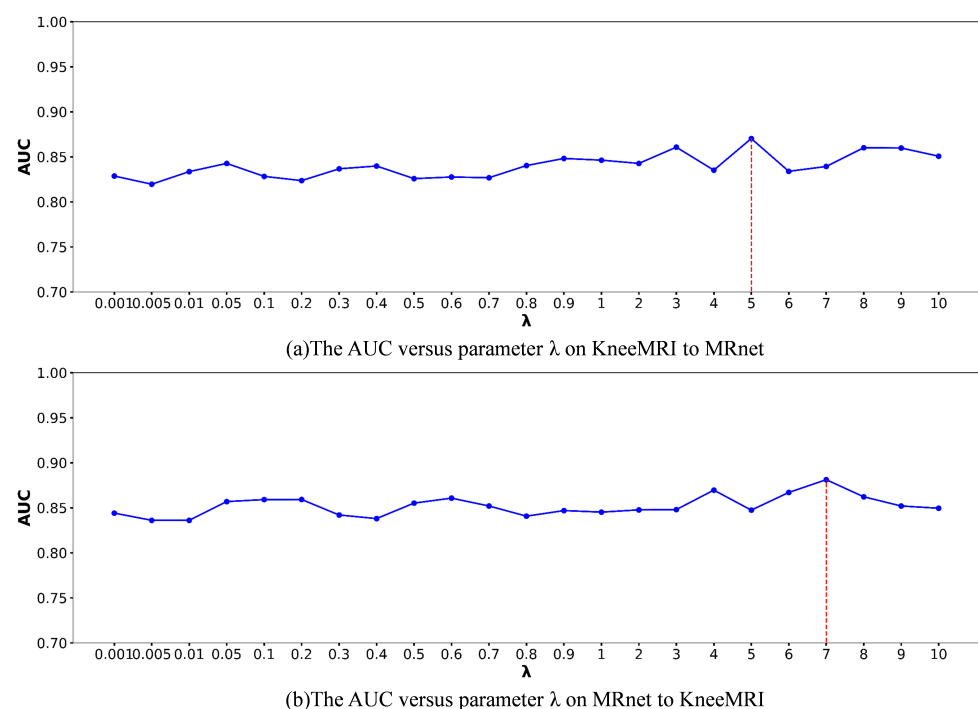


**Figure 9.** The AUC versus parameter  $\lambda$  in two tasks.

As illustrated in the charts, in the transfer learning from KneeMRI to MRnet, the AUC reached its optimum when  $\lambda$  was set to 5, while in the transfer learning from MRnet to KneeMRI, the AUC reached its optimum when  $\lambda$  was set to 7. The line graph indicates that the results exhibited minimal fluctuation, demonstrating the strong stability of our method.

Through comprehensive experimental testing of multiple hyperparameter configurations, we validated not only the effectiveness and robustness of our proposed method, but also generated significant reference data for future studies. These tests demonstrate the important impact of hyperparameter adjustment in improving model performance. Furthermore, our contrastive learning approach regularly maintains high accuracy and stability in a variety of configurations, proving its broad application and good generalization skills.

#### 4.3.3. Ablation Experiment Results Analysis

We conducted ablation experiments to validate the effectiveness of each module. The summarized results are presented in Tables 3 and 4. From these tables, it is evident that employing individual experimental methods alone may lead to a decrease in model performance. However, integrating the source domain filtering strategy with contrastive

learning noticeably enhances the model's performance. The following provides a detailed analysis of each part of the ablation experiments.

**Table 3.** Comparison of ablation experiments from KneeMRI to MRnet.

Source Data Filtering	Comparative Learning	AUC
		0.8447
✓		0.8310
	✓	0.8166
✓	✓	0.8703

**Table 4.** Comparison of ablation experiments from MRnet to KneeMRI.

Source Data Filtering	Comparative Learning	AUC
		0.8462
✓		0.8395
	✓	0.8502
✓	✓	0.8812

First, we performed an ablation experiment on source domain preprocessing in which contrastive learning was not used and the source domain data were simply filtered before being used directly in model training. According to the findings, the model's performance declined under these conditions, demonstrating that simply filtering the source domain data without further direction does not produce satisfactory results.

Next, we evaluated the impact of contrastive learning. Specifically, we discovered that the model's performance improved in the transfer learning from MRnet to KneeMRI but decreased in the transfer learning from KneeMRI to MRnet. This shows that contrastive learning, when used simply with positive and negative sample pairs, can produce contradictory results. As a result, filtering is critical for improving the data's representativeness.

These two experimental examples demonstrate that meaningful performance improvements can only be achieved when both contrastive learning for loss computation and source domain data filtering are used concurrently. This not only verifies the efficacy of our method, but also emphasizes the need to use proper tactics in domain transfer tasks. This integrated strategy allows the model to attain optimal performance and effective transfer across domains.

## 5. Discussion

In this research, we address the problem of limited generalization in transfer learning for ACL diagnostic models by putting forth a strategy that combines contrastive learning methods with source domain sample filtering methodologies. First, we apply various data preparation techniques that are specific to the properties of MRI data for the source and target regions. We iteratively modify the source domain training set by identifying mispredicted samples, which reveal feature space discrepancies that need to be adjusted, and fine-tuning the network. The target domain has a unique sample form; therefore, traditional contrastive learning methods are not immediately applicable. Rather, before training starts, we use the network to pre-extract features from the target domain training samples. We then build a loss function that combines contrastive loss and weighted classification loss for the source domain samples.

Our methodology's fundamental components extend beyond the KneeMRI and MRnet datasets. This approach can be used for various medical imaging applications that need transfer learning. For example, extending this method to different types of MRI scans, such as those used for brain or spine diagnoses, could illustrate its adaptability. It can also be applied to other imaging modalities, such as CT or PET scans, by tailoring the feature extraction and loss methods to the unique properties of each. Our method's flexibility



and adaptability suggest that it has the potential to increase model performance and generalization in a wide range of medical imaging applications.

Our strategy has substantial advantages over classic contrastive learning techniques and existing multimodal models. Traditional contrastive learning frequently employs a one-size-fits-all strategy that may neglect domain-specific difficulties, but our method pre-extracts characteristics from the target domain, better tailoring the model to its unique qualities. Furthermore, by integrating contrastive loss and weighted classification loss, our technique outperforms single-loss methods in terms of feature discrimination and sample distribution imbalance. Compared to multimodal models, which necessitate significant computational resources and big datasets, our method is more resource-efficient. It offers a practical solution by focusing on single-modality data while efficiently managing domain-specific features, making it especially useful in situations when multimodal data are limited or unavailable.

Contrastive learning has gained traction in the field of medical imaging, mainly due to its ability to learn robust feature representations from limited data. For example, in recent years, several studies have used contrastive learning to improve model generalization in various medical imaging tasks. Zhang et al. [34] demonstrated the use of contrastive learning in multimodal medical image segmentation, where they successfully improved segmentation accuracy by using unlabeled data to learn invariant features across different imaging modalities. Similarly, Ammar et al. [35] applied contrastive learning to cardiac MRI classification, which helped distinguish between different cardiac conditions by effectively managing class imbalances and improving feature discrimination.

However, our work adds significant changes that distinguish it from previous investigations. Unlike standard techniques, we extract features from target domain samples prior to performing contrastive learning, which is an essential adaption given the target domain's specific properties in ACL diagnosis. In addition, we combine the contrastive loss with a classification loss, which not only enhances feature discrimination but also tackles the issues caused by sample distribution imbalances between the source and target domains.

In conclusion, while contrastive learning is frequently employed, the unique changes in our methodology represent major advancements. A more in-depth review of the current literature would help to clarify the innovative components of our work, better situate it within the larger research landscape, and emphasize its significance for transfer learning in medical imaging.

Nevertheless, this study has limitations, prompting several avenues for future research:

1. Improving source domain data filtering procedures to ensure the accurate identification of samples that need adjustment, especially those that differ significantly from positive samples in the target domain.
2. Exploring more effective feature extraction techniques for target domain features to better align with real-time properties, potentially impacting the design of contrastive loss.
3. Refining contrastive loss calculation methods to better accommodate the one-to-many matching nature of source and target domain samples in contrastive learning.
4. Moving away from supervised learning approaches in the target domain and toward unsupervised learning methods that better represent real-world data issues in medical diagnostics.

These directions aim to advance the robustness and applicability of our proposed methodology in real-world medical imaging applications.

## 6. Conclusions

In this study, we introduce an innovative domain-adaptive transfer learning technique designed to enhance ACL damage identification between the KneeMRI and MRnet datasets. Our method incorporates a source domain filtering module to identify successful domain adaptation samples. In addition, we apply contrastive learning loss to address the difficulty of insufficient model generalization in the target domain due to small sample sizes. This

strategy establishes similarity links between the source and destination domains, which successfully guides domain adaptation model training.

The results of our bidirectional transfer learning experiments between the two datasets validate the efficacy of the proposed method. Specifically, the AUC improved from 0.845 to 0.870 in the transfer learning from KneeMRI to MRnet and from 0.846 to 0.881 in the transfer learning from MRnet to KneeMRI. These experimental findings demonstrate that combining contrastive learning with appropriate data processing techniques can greatly improve transfer learning tasks in medical image identification. Our findings suggest new applications for these approaches in medical diagnosis.

**Author Contributions:** Conceptualization, W.L. (Weiqiang Liu) and W.L. (Weilun Lin); methodology, W.L. (Weiqiang Liu) and W.L. (Weilun Lin); software, W.L. (Weilun Lin); validation, W.L. (Weiqiang Liu) and W.L. (Weilun Lin); formal analysis, W.L. (Weiqiang Liu); investigation, Z.Z.; resources, K.M.; data curation, W.L. (Weilun Lin); writing—original draft preparation, W.L. (Weiqiang Liu); writing—review and editing, W.L. (Weilun Lin) and Z.Z.; visualization, W.L. (Weilun Lin); supervision, Z.Z.; project administration, K.M.; funding acquisition, W.L. (Weiqiang Liu) and K.M. All authors have read and agreed to the published version of the manuscript.

**Funding:** This study was supported by China’s Education and Research Project of Young and Middle-aged Teachers of Fujian Province (under grant number JZ230032).

**Data Availability Statement:** The data we used were obtained from <https://stanfordmlgroup.github.io/projects/MRnet/> (accessed on 6 May 2024) and <http://www.riteh.uniri.hr/~istajduh/projects/kneeMRI/> (accessed on 20 May 2024).

**Acknowledgments:** The authors wish to thank the anonymous reviewers for their valuable suggestions.

**Conflicts of Interest:** The authors declare no conflicts of interest.

## References

1. Fox, A.J.S.; Wanivenhaus, F.; Burge, A.J.; Warren, R.F.; Rodeo, S.A. The human meniscus: A review of anatomy, function, injury, and advances in treatment. *Clin. Anat.* **2015**, *28*, 269–287. [\[CrossRef\]](#) [\[PubMed\]](#)
2. Zhang, L.; Liu, G.; Han, B.; Wang, Z.; Yan, Y.; Ma, J.; Wei, P. Knee joint biomechanics in physiological conditions and how pathologies can affect it: A systematic review. *Appl. Bionics Biomech.* **2020**, *2020*, 7451683. [\[CrossRef\]](#) [\[PubMed\]](#)
3. Beaulieu, M.L.; Ashton-Miller, J.A.; Wojtys, E.M. Loading mechanisms of the anterior cruciate ligament. *Sport. Biomech.* **2023**, *22*, 1–29. [\[CrossRef\]](#) [\[PubMed\]](#)
4. Logterman, S.L.; Wydra, F.B.; Frank, R.M. Posterior cruciate ligament: Anatomy and biomechanics. *Curr. Rev. Musculoskelet. Med.* **2018**, *11*, 510–514. [\[CrossRef\]](#)
5. Lim, W.L.; Liao, L.L.; Ng, M.H.; Chowdhury, S.R.; Law, J.X. Current progress in tendon and ligament tissue engineering. *Tissue Eng. Regen. Med.* **2019**, *16*, 549–571. [\[CrossRef\]](#) [\[PubMed\]](#)
6. Kaeding, C.C.; Léger-St-Jean, B.; Magnussen, R.A. Epidemiology and diagnosis of anterior cruciate ligament injuries. *Clin. Sport. Med.* **2017**, *36*, 1–8. [\[CrossRef\]](#) [\[PubMed\]](#)
7. Herzog, M.M.; Marshall, S.W.; Lund, J.L.; Pate, V.; Mack, C.D.; Spang, J.T. Trends in incidence of ACL reconstruction and concomitant procedures among commercially insured individuals in the United States, 2002–2014. *Sport. Health* **2018**, *10*, 523–531. [\[CrossRef\]](#) [\[PubMed\]](#)
8. Chia, L.; Silva, D.D.O.; Whalan, M.; McKay, M.J.; Sullivan, J.; Fuller, C.W.; Pappas, E. Non-contact anterior cruciate ligament injury epidemiology in team-ball sports: A systematic review with meta-analysis by sex, age, sport, participation level, and exposure type. *Sport. Med.* **2022**, *52*, 2447–2467. [\[CrossRef\]](#) [\[PubMed\]](#)
9. Tan, S.H.S.; Lau, B.P.H.; Khin, L.W.; Lingaraj, K. The importance of patient sex in the outcomes of anterior cruciate ligament reconstructions: A systematic review and meta-analysis. *Am. J. Sports Med.* **2016**, *44*, 242–254. [\[CrossRef\]](#)
10. Filbay, S.; Culvenor, A.; Ackerman, I.; Russell, T.; Crossley, K. Quality of life in anterior cruciate ligament-deficient individuals: A systematic review and meta-analysis. *Br. J. Sport. Med.* **2015**, *49*, 1033–1041. [\[CrossRef\]](#)
11. Filbay, S.R.; Ackerman, I.N.; Russell, T.G.; Macri, E.M.; Crossley, K.M. Health-related quality of life after anterior cruciate ligament reconstruction: A systematic review. *Am. J. Sports Med.* **2014**, *42*, 1247–1255. [\[CrossRef\]](#) [\[PubMed\]](#)
12. Filbay, S.R.; Crossley, K.M.; Ackerman, I.N. Activity preferences, lifestyle modifications and re-injury fears influence longer-term quality of life in people with knee symptoms following anterior cruciate ligament reconstruction: A qualitative study. *J. Physiother.* **2016**, *62*, 103–110. [\[CrossRef\]](#) [\[PubMed\]](#)
13. Lee, S.H.; Yun, S.J. Efficiency of knee ultrasound for diagnosing anterior cruciate ligament and posterior cruciate ligament injuries: A systematic review and meta-analysis. *Skelet. Radiol.* **2019**, *48*, 1599–1610. [\[CrossRef\]](#)

14. Liu, D.; Hu, P.; Cai, Z.J.; Lu, W.H.; Pan, L.Y.; Liu, X.; Peng, X.J.; Li, Y.S.; Xiao, W.F. Valid and reliable diagnostic performance of dual-energy CT in anterior cruciate ligament rupture. *Eur. Radiol.* **2023**, *33*, 7769–7778. [[CrossRef](#)] [[PubMed](#)]
15. Zhao, M.; Zhou, Y.; Chang, J.; Hu, J.; Liu, H.; Wang, S.; Si, D.; Yuan, Y.; Li, H. The accuracy of MRI in the diagnosis of anterior cruciate ligament injury. *Ann. Transl. Med.* **2020**, *8*, 1657. [[CrossRef](#)] [[PubMed](#)]
16. Sun, J.; Wang, L.; Razmjoooy, N. Anterior cruciate ligament tear detection based on deep belief networks and improved honey badger algorithm. *Biomed. Signal Process. Control* **2023**, *84*, 105019. [[CrossRef](#)]
17. Zhang, M.; Huang, C.; Druzhinin, Z. A new optimization method for accurate anterior cruciate ligament tear diagnosis using convolutional neural network and modified golden search algorithm. *Biomed. Signal Process. Control* **2024**, *89*, 105697. [[CrossRef](#)]
18. Chan, S.; Zhang, M.; Zhi, Y.Y.; Razmjoooy, S.; El-Sherbeeney, A.M.; Lin, L. Improved anterior cruciate ligament tear diagnosis using gated recurrent unit networks and Hybrid Tasmanian Devil Optimization. *Biomed. Signal Process. Control* **2024**, *95*, 106309. [[CrossRef](#)]
19. Santone, A.; Cesarelli, M.; Colasuonno, E.; Bevilacqua, V.; Mercaldo, F. A Method for Ocular Disease Diagnosis through Visual Prediction Explainability. *Electronics* **2024**, *13*, 2706. [[CrossRef](#)]
20. Gago-Fabero, Á.; Muñoz-Saavedra, L.; Civit-Masot, J.; Luna-Perejón, F.; Rodríguez Corral, J.M.; Domínguez-Morales, M. Diagnosis Aid System for Colorectal Cancer Using Low Computational Cost Deep Learning Architectures. *Electronics* **2024**, *13*, 2248. [[CrossRef](#)]
21. Kao, Y.H.; Lin, C.L. Enhancing Diabetic Retinopathy Detection Using Pixel Color Amplification and EfficientNetV2: A Novel Approach for Early Disease Identification. *Electronics* **2024**, *13*, 2070. [[CrossRef](#)]
22. Liu, X.; Zhu, X.; Tian, X.; Iwasaki, T.; Sato, A.; Kazama, J.J. Renal Pathological Image Classification Based on Contrastive and Transfer Learning. *Electronics* **2024**, *13*, 1403. [[CrossRef](#)]
23. Bien, N.; Rajpurkar, P.; Ball, R.L.; Irvin, J.; Park, A.; Jones, E.; Bereket, M.; Patel, B.N.; Yeom, K.W.; Shpanskaya, K.; et al. Deep-learning-assisted diagnosis for knee magnetic resonance imaging: Development and retrospective validation of MRNet. *PLoS Med.* **2018**, *15*, e1002699. [[CrossRef](#)] [[PubMed](#)]
24. Štajduhar, I.; Mamula, M.; Miletić, D.; Uenal, G. Semi-automated detection of anterior cruciate ligament injury from MRI. *Comput. Methods Programs Biomed.* **2017**, *140*, 151–164. [[CrossRef](#)] [[PubMed](#)]
25. Javed Awan, M.; Mohd Rahim, M.S.; Salim, N.; Mohammed, M.A.; Garcia-Zapirain, B.; Abdulkareem, K.H. Efficient detection of knee anterior cruciate ligament from magnetic resonance imaging using deep learning approach. *Diagnostics* **2021**, *11*, 105. [[CrossRef](#)] [[PubMed](#)]
26. Tsai, C.H.; Kiryati, N.; Konen, E.; Eshed, I.; Mayer, A. Knee injury detection using MRI with efficiently-layered network (ELNet). In Proceedings of the Medical Imaging with Deep Learning, PMLR, Montreal, QC, Canada, 6–8 July 2020; pp. 784–794.
27. Dunnhofer, M.; Martinel, N.; Micheloni, C. Improving MRI-based knee disorder diagnosis with pyramidal feature details. In Proceedings of the Medical Imaging with Deep Learning, PMLR, Lübeck, Germany, 7–9 July 2021; pp. 131–147.
28. Belton, N.; Welaratne, I.; Dahlan, A.; Hearne, R.T.; Hagos, M.T.; Lawlor, A.; Curran, K.M. Optimising knee injury detection with spatial attention and validating localisation ability. In Proceedings of the Annual Conference on Medical Image Understanding and Analysis, Aberdeen, UK, 19–21 July 2021; Springer: Berlin/Heidelberg, Germany, 2021; pp. 71–86. [[CrossRef](#)]
29. van Opbroek, A.; Achterberg, H.C.; Vernooij, M.W.; Ikram, M.A.; de Bruijne, M.; Initiative, A.D.N. Transfer learning by feature-space transformation: A method for Hippocampus segmentation across scanners. *NeuroImage Clin.* **2018**, *20*, 466–475. [[CrossRef](#)] [[PubMed](#)]
30. Zhang, Y.; An, M. Deep learning-and transfer learning-based super resolution reconstruction from single medical image. *J. Healthc. Eng.* **2017**, *2017*, 5859727. [[CrossRef](#)] [[PubMed](#)]
31. Cheng, B.; Liu, M.; Zhang, D.; Munsell, B.C.; Shen, D. Domain transfer learning for MCI conversion prediction. *IEEE Trans. Biomed. Eng.* **2015**, *62*, 1805–1817. [[CrossRef](#)] [[PubMed](#)]
32. He, K.; Zhang, X.; Ren, S.; Sun, J. Deep residual learning for image recognition. In Proceedings of the IEEE Conference on Computer Vision and Pattern Recognition, Las Vegas, NV, USA, 27–30 June 2016; pp. 770–778. [[CrossRef](#)]
33. Hu, F.; Chen, A.A.; Horng, H.; Bashyam, V.; Davatzikos, C.; Alexander-Bloch, A.; Li, M.; Shou, H.; Satterthwaite, T.D.; Yu, M.; et al. Image harmonization: A review of statistical and deep learning methods for removing batch effects and evaluation metrics for effective harmonization. *NeuroImage* **2023**, *274*, 120125. [[CrossRef](#)]
34. Zhang, J.; Zhang, S.; Shen, X.; Lukasiewicz, T.; Xu, Z. Multi-ConDoS: Multimodal contrastive domain sharing generative adversarial networks for self-supervised medical image segmentation. *IEEE Trans. Med. Imaging* **2023**, *43*, 76–95. [[CrossRef](#)]
35. Ammar, A.; Bouattane, O.; Youssfi, M. Automatic cardiac cine MRI segmentation and heart disease classification. *Comput. Med Imaging Graph.* **2021**, *88*, 101864. [[CrossRef](#)] [[PubMed](#)]

**Disclaimer/Publisher’s Note:** The statements, opinions and data contained in all publications are solely those of the individual author(s) and contributor(s) and not of MDPI and/or the editor(s). MDPI and/or the editor(s) disclaim responsibility for any injury to people or property resulting from any ideas, methods, instructions or products referred to in the content.